Energy Proceedings
Vol 26, 2022
ISSN 2004-2965

Numerical Investigation of Heat Transfer and Pressure Drop Characteristics of Mango Bark-CO_2 Nanofluid in inclined Gas Cooling Process

Uwadoka O[1], Adelaja AO[1*], Noah OO[1], Fadipe OL[2**], Lee SW[2]

1 Department of Mechanical Engineering, University of Lagos, Akoka, Yaba, Lagos State, 101017, Nigeria

2 Department of Industrial and Systems Engineering, Morgan State University, 1700 East Cold Spring Lane, Baltimore, Maryland

* Corresponding Author: aadelaja@unilag.edu.ng

** Alternative Corresponding Author: opfad1@morgan.edu

ABSTRACT

This paper investigates the heat transfer and pressure drop characteristics of mango bark-CO_2 nanofluid. The physical model comprises flow in a pipe under a constant heat flux of -10W/m^2. The inclination angle varies between -90^o and +90^o, and volume fraction between 0% and 2.0% for Reynolds numbers of 50 and 100. The numerical code is validated using three research studies on heat transfer coefficient, Nusselt number, and pressure drop. Results show that the heat transfer coefficient and pressure increase with nanofluid volume concentration and Reynolds number. However, the heat transfer coefficient varies nonlinearly with the inclination angle and has a maximum occurring when the inclination angles are -30^o and +60^o while the pressure drop is relatively constant.

Keywords: Mango bark-CO_2 nanofluid, heat transfer coefficient, pressure drop, inclination angle, smooth circular tube

NOMENCLATURE

Abbreviations	
ODP	Ozone Depletion Potential
GWP	Global Warming Potential
Symbols	
ρ	Density
C_p	Specific heat at constant pressure
k	Thermal Conductivity
μ	Viscosity
T	Temperature
h	Heat transfer coefficient
q	Heat flux
Nu	Nusselt number
$\vec{v}$	Velocity vector
Subscripts	
nf	Nanofluid
p	Particle
f	Base fluid
b	Bulk
in	Inlet
out	Outlet

1. INTRODUCTION

In both developed and developing countries, the demand for heat exchangers for heating and cooling purposes increases along with population and standard of living. Global energy consumption also grows exponentially due to this increase in demand. The major concern is that fuel usage and energy generation are directly linked to global warming and the greenhouse gas effects (i.e., the discharge of CO_2 into the atmosphere). Also, the conventional refrigerants used in heat exchange equipment are harmful to the environment due to their high Ozone-depleting potentials (ODP) and global warming potentials (GWP).

A study by Lorentzen and Pettersen [1] proposed the resurgence of CO_2 as an eco-friendly refrigerant to solve the climate change challenges. However, Groll and Kim [2] reported that CO_2 had unfavorable thermodynamic characteristics, such as a low critical temperature and a higher working pressure, making it unsuitable for use in a typical vapour compression system compared to other non-synthetic refrigerants. Their study corroborated Pérez-García et al. [3], who reported that the inefficiency of CO_2 as a refrigerant was due to the losses in the expansion stage of refrigeration. However, gas coolers have been significantly used in commercial refrigeration cooling technologies.

Choi and Eastman [4] were the first in the open literature to discuss nanofluids. Since then, numerous papers have reported increasing the thermal efficiencies

of nanofluid-based heat exchangers. One of these was a report by Wu et al. [5], which examined the pool boiling heat transmission of R11 refrigerant mixed with TiO_2 nanoparticles and found that at a volume fraction of 0.01 g/L, the heat transfer augmentation reached 20%. Sarkar [6] evaluated the effectiveness of Al_2O_3-water, TiO_2-water, CuO-water, and Cu-water for cooling a CO_2 gas cooler and noted the superiority of Al_2O_3 over the other nanofluids. Purohit et al. [7] studied the performance of Al_2O_3-water nanofluids for cooling a trans-critical CO_2 refrigeration system, and it was concluded that Al_2O_3 gave a better performance than water. However, typical mineral or metallic nanoparticle materials threaten the environment as they do not quickly decompose when disposed of, hence the need for bio-nanofluids.

In an attempt to study bio-nanofluid characteristics, Onyiriuka et al. [8] investigated the thermal characteristics of mango bark-water nanofluid in the horizontal in-tube heat exchanger. It was noted that there was an enhancement in the thermal performance of the nanofluid compared with water. Sharifpur et al. [9] also investigated the thermal conductivity of water and mango bark/water nanofluid at varying concentrations (0.1 percent, 0.5 percent, and 1.0 percent) and temperatures between 10°C and 40°C. Compared to water, the mango bark/water nanofluid had no appreciable thermal conductivity increase. Chen et al. [10] showed that palm kernel/water-EG and mango/water nanofluids had relatively low thermal conductivities compared to non-bio nanofluids and that hybrid non-bio nanofluids had the highest thermal conductivity for low nanoparticle concentration of 0.1%.

From the literature reviewed, it has been shown that no research has been done on mango bark-CO_2 nanofluid as an alternative to a CO_2 gas cooler for a more efficient heat exchange system. Also, the investigation of the effect of inclination angle on the mango bark-CO_2 nanofluid is scarce in the open literature. This paper, therefore, addresses these gaps using a numerical approach - ANSYS-Fluent software – to study the thermal and hydraulic characteristics of mango bark-CO_2 nanofluid in a gas cooler.

2. MATERIALS AND METHODS

2.1 Model description & methodology

Mango bark-CO_2 nanofluid at an initial temperature of 320K flows through a cylindrical pipe with an internal diameter of 4.5 mm and a length of 970mm. The pipe wall is exposed to a heat flux of -10W/m^2, as seen in Fig. 1. The flow is laminar and incompressible with Reynolds numbers of 50 and 100. The inclination angles are ±90°, ±60°, ±45°, ±30°, and 0°; and volume fractions are 0.5%, 1.0%, and 2.0%.

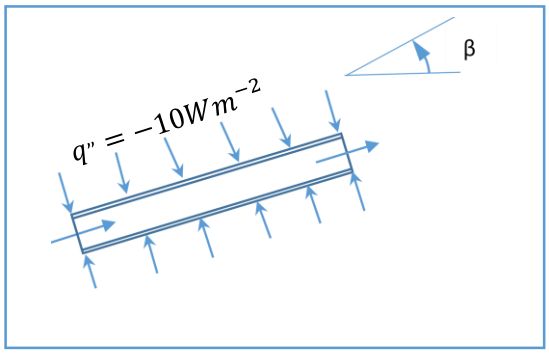

Fig. 1 Representation of the model

2.2 Governing Equations

The present study is a steady-state, three-dimensional one-phase flow. The thermal properties of the fluid for each case are kept constant. The conservations equations are as follows:

$$\nabla . \vec{v} = 0 \quad (1)$$

$$\rho_f(\vec{v}.\nabla\vec{v}) = -\nabla p + \rho_f \vec{g} cos\beta + \mu_f \nabla^2 \vec{v} \quad (2)$$

$$(\rho C_p)_f(\vec{v}\nabla T) = k_f \nabla^2 T \quad (3)$$

The energy equation for a solid body is:

$$k_s \nabla^2 T = 0 \quad (4)$$

where

k_s = 398 Wm^{-1}K^{-1} for copper - the solid structure.

The boundary condition at the solid-fluid interface is:

$$k_s \left.\frac{\partial T}{\partial n}\right| = k_f \left.\frac{\partial T}{\partial n}\right| \quad (5)$$

The channel wall no-slip condition is:

$$\vec{v} = 0 \quad (6)$$

The inlet temperature and pressure boundary conditions are expressed as:

$$T = T_{in} \quad (7)$$

$$p_{out} = p_{amb} \quad (8)$$

The solid-body external boundaries,

$$q = -10\ Wm^2 \quad (9)$$

2.3 Thermophysical properties

The properties of the nanofluid; relating to the nanoparticle and base fluid properties, can be expressed by Maxwell's relation as follows:

$$\rho_{nf} = \varphi\ \rho_p + (1-\varphi)\rho_f \quad (10)$$

Where ρ_{nf}, ρ_p, ρ_f and φ are the densities of the nanofluids, nanoparticles, base fluid, and volume fraction, respectively.

$$\mu_{nf} = \mu_f(1 + 2.8\ \varphi) \quad (11)$$

Where μ_{nf} and μ_f are the dynamic viscosities of the nanofluid and base fluid, respectively.

$$C_{p\,nf} = \frac{\varphi\ \rho_p\ C_{p\,p} + (1-\varphi)\rho_f\ C_{p\,f}}{\rho_{nf}} \quad (12)$$

Where $C_{p\,nf}$, C_{pp} and $C_{p\,f}$ are the specific heat capacities of the nanofluid, nanoparticle, and base fluid.

$$k_{nf} = k_f \left(\frac{k_p + 2\,k_f - 2\,\varphi\,(k_f - k_p)}{k_p + 2\,k_f + \varphi\,(k_f - k_p)} \right) \quad (13)$$

Where k_{nf}, k_p and k_f are the thermal conductivities of the nanofluid, nanoparticle, and base fluid, respectively.

2.4 Heat transfer coefficient calculations

The heat transfer coefficient can be calculated:

$$h = \frac{q}{T_w - T_f} \quad (14)$$

where q, T_w, and T_f are the heat flux, wall, and bulk fluid temperatures, respectively.

2.5 Pressure drop estimation

The pressure drop across the pipe was calculated from the difference between the upstream (p_{in}) and downstream (p_{out}) pressures of the channel. The relation for the pressure drop is given as:

$$\Delta p = p_{in} - p_{out} \quad (15)$$

3 MODEL VALIDATION

3.1 Error analyses

Experimental and numerical results were compared using the mean square error (MSE), root mean square error (RMSE), and the mean absolute deviation (MAD), given by the following relations:

$$MSE = \frac{1}{N}\sum_{i=1}^{N}(x_i - \hat{x}_i)^2 \quad (16)$$

$$RMSE = \sqrt{\frac{1}{N}\sum_{i=1}^{N}(x_i - \hat{x}_i)^2} \quad (17)$$

$$MAD = \frac{1}{N}\sum_{i=1}^{N}\frac{|x_i - \hat{x}_i| * 100}{\hat{x}_i} \quad (18)$$

Where N is the number of entries, X_i is the experimental value from other studies, and $\hat{X}_i$ is the predicted value from the numerical investigation.

3.2 Grid independence analysis

The most suitable mesh was determined by computing across a series of finite volume meshes with a varying number of grids. This was conducted using pure water, with a Reynolds number of 1050, as the fluid in the pipe. The outlet temperature was monitored to test the grid independence of the different mesh element sizes, as shown in Table 1. The test was carried out until the criterion of $\left|\frac{T_i - T_{i-1}}{T_i}\right| \leq 1\%$ was satisfied. The deviation between mesh numbers 5 and 6 is 0.79%. All simulations done in this study had the same mesh consistency as Mesh number 5. It was also observed that further increment in the number of meshes after Mesh number 6 led to non-convergence of results.

Table 1 Grid Independence Analysis

Mesh Number	Number of Meshes	Outlet Wall Temperature (K)	Deviation from Previous Grid
1	19499	314.61	---------
2	38597	321.9	2.32%
3	59941	340.202	5.69%
4	101166	335.057	1.51%
5	234971	329.626	1.62%
6	301534	327.024	0.79%

3.3 Validation

The dependency and accuracy of the simulation setup and code were validated before carrying out the investigation using the mango bark-CO_2 nanofluid. The model was validated using Shah's [11] equation, experimental investigations of Wen and Ding [12] on the heat transfer of water, convective heat transfer studies of Cu/Water nanofluids by Heris et al. [13], and convective heat transfer and pressure drop of Cu/Water Nanofluid by Nourafkan et al. [14].

Table 2 shows the error analyses between the current and validated studies. The largest value for the mean absolute deviation can be seen with Shah's equation at 31.45%. The significant error may be because Shah's equation was modeled for pipes of larger diameters. The mean absolute deviation for all other studies is less than 20%. Figs. 2 and 3 show the plots comparing the current and the validated studies.

4 RESULTS AND DISCUSSIONS

4.1 Effect of inclination angle on heat transfer coefficient

The heat transfer coefficient as a function of the inclination angle for different volume fractions for Reynolds numbers of 50 and 100 are presented in Figs. 4 and 5. The heat transfer coefficient and inclination angle for both Reynolds numbers are similar. The results indicate that the heat transfer coefficient increases with nanofluid volume fraction and Reynolds number due to the increased molecular inter-collision and the Brownian motion. For both cases, the 2.0% vol. fraction nanofluid gives the highest heat transfer coefficient, typical for most nanofluids. With inclination angle, the heat transfer

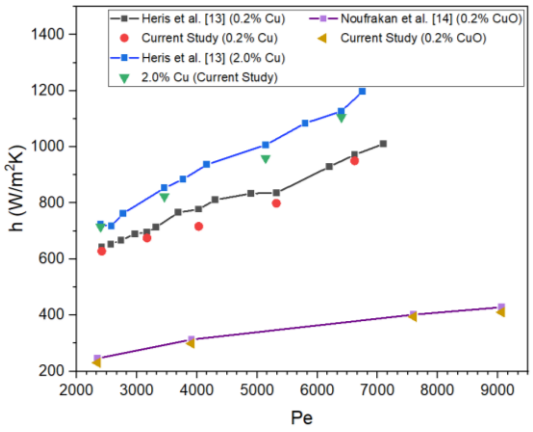

Fig. 2 Comparison of the present study for Heat Transfer coefficient with the experimental result of a) Heris et al. [13] and b) Noufrakan et al. [14]

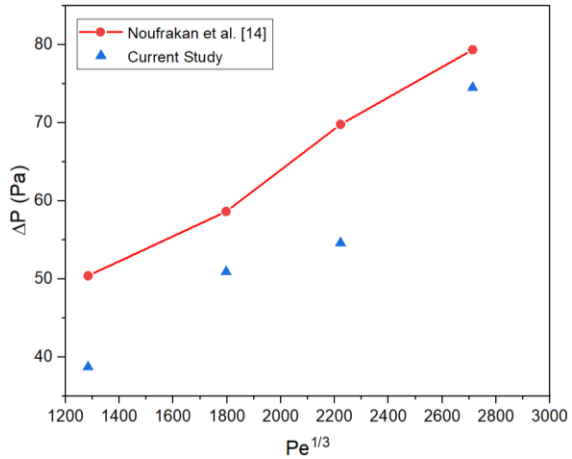

Fig. 3 Comparison of the present study for Pressure Drop with the experimental result of Noufrakan et al. [14]

coefficient increases from -90°, peaks at -30°, reduces to a low at 0°, and peaks again at +60° before decreasing to another low at +90°. This variation may be due to the effect of gravitational force on the thermal boundary layer as the angle changes. The highest values occur at -30° and +60°, while the lowest values occur at ±90° and 0°.

4.2 Effect of inclination angle on pressure drop

Figs. 6 and 7 show the effect of inclination on the pressure drop for the Reynolds number of 50 and 100. Results show that pressure drop increases with nanofluid volume fraction and Reynolds number but is not very significant with variation in the inclination angle. The volume fractions of 2.0 % vol. fraction possess the highest value. This may be attributed to the nanofluid's increased viscosity and density, which increase with the vol. fraction. The density and viscosity strongly influence the pressure drop across the flow.

5 CONCLUSION

A numerical investigation of the heat transfer and

Table 2 Error measurements for validated studies

Study Validated	Parameters	MSE	RMSE	MAD (%)
Shah [11]	Nu vs. x/D (Water)	2.745	1.657	31.450
Wen and Ding [12]	Nu vs. Re (Water)	3.412	1.847	13.990
Heris et al. [13]	h vs. Pe (0.2% Cu/Water Nanofluid)	1440.526	37.954	4.110
	h vs. Pe (2.0% Cu/Water Nanofluid)	896.567	29.943	2.885
Nourafkan et al. [14]	h vs. Pe (0.2% CuO/Water Nanofluid)	447.542	21.160	5.352
	ΔP vs. Pe^1/3 (2.0% CuO/Water Nanofluid)	112.883	10.620	19.953

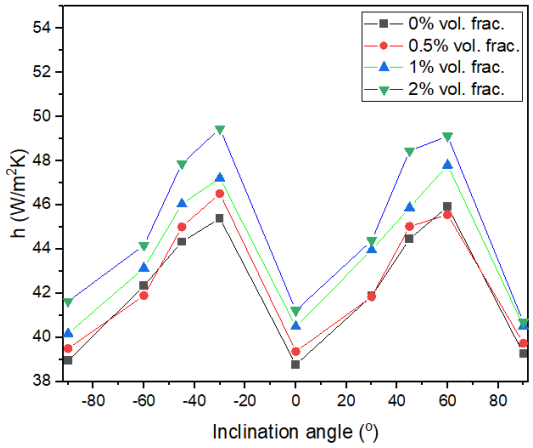

Fig. 4 Heat transfer coefficient vs. inclination angle for Re = 50

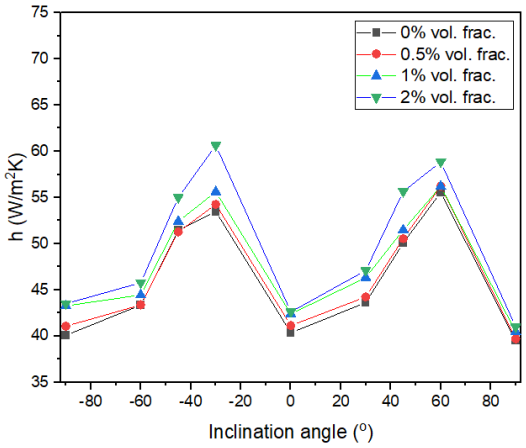

Fig. 5 Heat transfer coefficient vs. inclination angle for Re = 100

pressure drop characteristics of mango bark/CO_2 nanofluid through a circular pipe is carried out. The numerical simulation is carried out using ANSYS Fluent. The effect of the inclination angle, nanofluid volume fraction, and Reynolds number are investigated on the heat transfer coefficient and pressure drop. An increase in Reynolds number and nanofluid volume fraction increases the heat transfer coefficient and pressure drop. However, the inclination angle variation

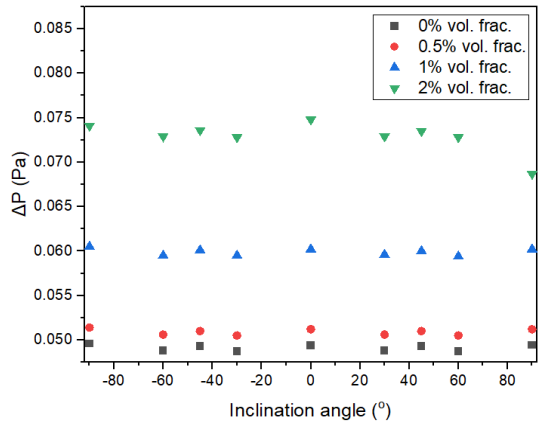

Fig. 6 Pressure drop vs. inclination angle for Re = 50

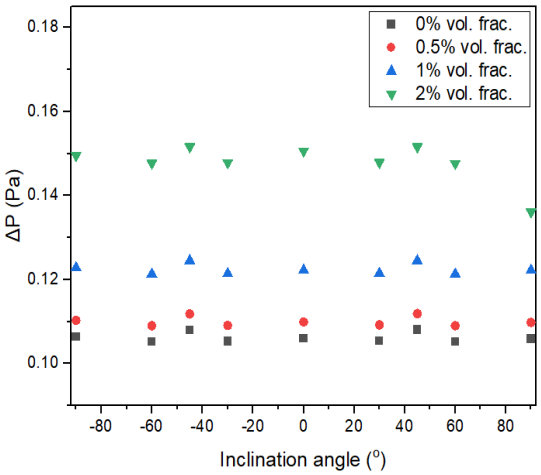

Fig. 7 Pressure drop vs. inclination angle for Re = 100

significantly influences only the heat transfer coefficient as the pressure drop is relatively constant. The highest heat transfer coefficient is noted for the inclination angles of -30° and +60°.

ACKNOWLEDGEMENT

The authors appreciate the support from the University of Lagos, Nigeria, and Morgan State University, Maryland, USA, to present this paper at ICAE2022.

REFERENCES

[1] Lorentzen G, Pettersen J. A new efficient and environmentally benign system for car air-conditioning. Int J Refrig 1993;16(1): 4-12.

[2] Groll EA, Kim J. Review Article: Review of Recent Advances toward Transcritical CO_2 Cycle Technology. HVAC&R Res 2007; 499 – 520.

[3] Pérez-García V, Belman-Flores JM, Navarro-Esbrí J, Rubio-Maya C. Comparative study of transcritical vapor compression configurations. Appl Therm Eng 2013;51(1-2): 1038-1046.

[4] Choi S, Eastman JA. Enhancing thermal conductivity of fluids with nanoparticles. United States,1995

[5] Wu Li, XM, Li, P. Investigation of pool boiling heat transfer of R11 with TiO_2 nanoparticle. J Eng Thermophys 2008;28.

[6] Sarkar J. Performance improvement of double-tube gas cooler in a CO2 refrigeration system using nanofluids. Therm Sci 2015;19 (1): 109-118.

[7] Purohit N, Khangarot BS, Gullo P, Purohit K, Dasgupta MS. Assessment of alumina nanofluid as a coolant in double pipe gas cooler for trans-critical CO_2 refrigeration cycle. Energy Procedia 2017;109: 219 –226.

[8] Onyiriuka EJ, Ighodaro OO, Adelaja AO, Ewim DRE, Bhattacharyya S. A numerical investigation of the heat transfer characteristics of water-based mango bark nanofluid flowing in a double-pipe heat exchanger. Heliyon 2019;5: e02416

[9] Sharifpur M, Solomon A, Meyer JP, Ibrahim J, Immanuel B. Thermal Conductivity and Viscosity of Mango Bark / Water Nanofluids. 13th International Conference on Heat Transfer, Fluid Mechanics and Thermodynamics. Portorož, Slovenia 2017.

[10] Chen J, Oumer A, Azizuddin A. A review on thermo-physical properties of bio, non-bio and hybrid nanofluids. Journal of Mechanical Engineering and Sciences 2019; 13(4): 5875-5904.

[11] Shah R. Thermal entry length solutions for the circular tube and parallel plates. Proceedings of 3rd National Heat and Mass Transfer Conference 1975;1: 11-75. Bombay: Indian Institute of Technology.

[12] Wen D, Ding Y. Experimental investigation into convective heat transfer of nanofluids at the entrance region under laminar flow conditions. Int J Heat Mass Transf 2004;47(24): 5181–5188.

[13] Heris S, Etemad SG, Esfahany MN. Convective Heat Transfer of a Cu/Water Nanofluid Flowing Through a Circular Tube. Exp Heat Transf 2009; 22(4): 217-227.

[14] Nourafkan E, Karimi G, Moradgholi J. Experimental Study of Laminar Convective Heat Transfer and Pressure Drop of Cuprous Oxide/Water Nanofluid Inside a Circular Tube. Exp Heat Transf 2015;28(1): 58-68.